Int. J. Heat Mass Transfer. Vol. 29, No. 2, pp. 215–225, 1986
Printed in Great Britain

0017–9310/86 $3.00 + 0.00

A study of heat transfer during arc welding

M. SALCUDEAN,* M. CHOI† and R. GREIF†

* University of Ottawa, Department of Mechanical Engineering, Ottawa, Ontario, Canada
† University of California, Berkeley, Department of Mechanical Engineering, Berkeley, CA 94720, U.S.A.

(*Received* 29 *January* 1985 *and in final form* 29 *July* 1985)

Abstract—An analysis of heat transfer during welding has been carried out. The heat transfer mechanisms considered include conduction, solid–liquid phase change, liquid–vapor phase change and radiation. The penetration depth is calculated for different power levels and distributions and the results are compared with experimental data for lead. The contributions and the importance of the different heat transfer modes are assessed.

1. HEAT TRANSFER DURING WELDING

UNDERSTANDING of the heat transfer during welding is of considerable practical significance since pool shape, thermal stresses, heat losses, etc. significantly affect weld quality and productivity [1–3]. The phenomena are complex and unsteady and involve the source of the power as well as melting, solidification, vaporization, thermal radiation and convection effects. The present study emphasizes stationary gas tungsten arc welding. Weld modeling calculations have been carried out for this process [1–3] including recent contributions and reviews by, e.g. Glickstein and Friedman [4, 5] and Landram [6].

The goal of the present work is the study of the heat transfer mechanisms during arc welding. The heat transfer modes include conduction, solid–liquid phase change, liquid–vapor phase change and radiation. A spherical configuration is considered as shown in Fig. 1. Convection in the weld pool is neglected [6]. Radial and colatitude variations are permitted and azimuthal symmetry is assumed. The basic equations and the corresponding boundary conditions are expressed in finite-difference form. The equations are solved using two different methods: an explicit method and an Alternating Direction Implicit (ADI) method. Lead was chosen for extensive evaluation of the model because of the following considerations:

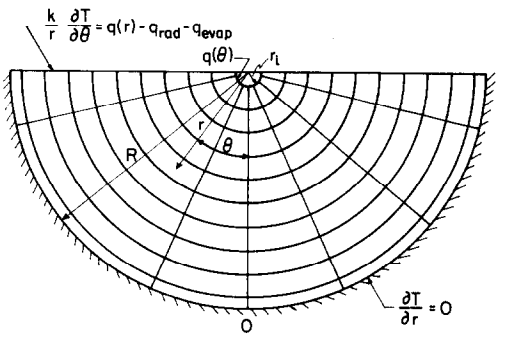

FIG. 1. Sketch of hemisphere.

1. Lead has a low boiling temperature and consequently significant loss of material occurs during welding. This adds to the complexity of the phenomena and broadens the applicability of the analysis to include both low and high fusion temperature materials.
2. The extensive availability of data.

Subsequent studies will include other metals.

The computations were carried out for different power levels and different heat input distributions. The resulting temperature field, fusion boundary penetration and heat transfer in the various modes are presented, and the results are analyzed and compared with experimental data.

Landram [6] has carried out extensive investigations for the determination of the fusion boundary energy transport during arc welding. He has made temperature measurements on the boundary during the welding process and has identified fusion boundary transport mechanisms by applying an inverse conduction method.

2. PHYSICAL MODEL AND MATHEMATICAL FORMULATION

The magnitude and distribution of the heat input from the welding arc are required for the thermal analysis of a weld. Two different distributions for the surface heat flux have been considered: one corresponds to a concentrated 'point' source [7] and the other corresponds to a Gaussian distribution [4, 5]. In this study several distributions, some slight modifications of the above, are used.

The magnitude of the total input, Q, is given by $Q = \eta EI$ where η is the arc efficiency, E is the arc voltage and I is the arc current. This power is assumed to be independent of time. The determination of the arc efficiency is an essential consideration in analyzing the heat transfer during welding. In this study the arc efficiency was a parameter which was approximated based on the calculations of the fusion boundary power using Landram's data [6].

NOMENCLATURE

A, B, C coefficients [equation (7)] for lead; 10.69, 9600, −3.0758
c_p specific heat
E arc voltage
h_{fg}, h_{fus} latent heat of vaporization and fusion
I arc current
k thermal conductivity
Δm mass loss
Q total input power
$q(r)$ heat flux outside cavity
$q(\theta)$ heat flux over the cavity
q_{evap}, q_{rad} heat loss due to evaporation and radiation
R radius of weldment
$r, \Delta r$ radius and radius increment
r_{ch} characteristic radius
T temperature
T_{boil}, T_{melt} temperatures of boiling and melting
$t, \Delta t$ time and time increment
ΔV element volume
W evaporation flux.

Greek symbols
δ penetration depth
ε total emissivity
η arc efficiency
$\theta, \Delta\theta$ angle and angle increment
ρ density.

Subscripts
i initial condition
i, j node indexes
l liquid
s solid, surface
∞ ambient.

Superscripts
$n, n+1/2, n+1$ time level index.

2.1. The following heat distributions were studied.

(a) Concentrated heat flux acting uniformly over a small cavity [cf. Fig. 2, case (a)]. In this case, the heat input is considered to act in a concentrated manner, like a point source, and the resulting flux is assumed to be distributed uniformly over the small cavity. This can be considered to be a model of a point heat source.

(b) Concentrated heat flux acting non-uniformly over a small cavity [cf. Fig. 2, case (b)]. The flux is assumed to have a cosine variation over the small cavity surface with the total power equal to that for the uniform heat flux of case (a). The heat flux is a maximum at $\theta = 0°$.

(c) Distributed heat flux acting over a large flat surface without a cavity [cf. Fig. 2, case (c)]. The heat flux

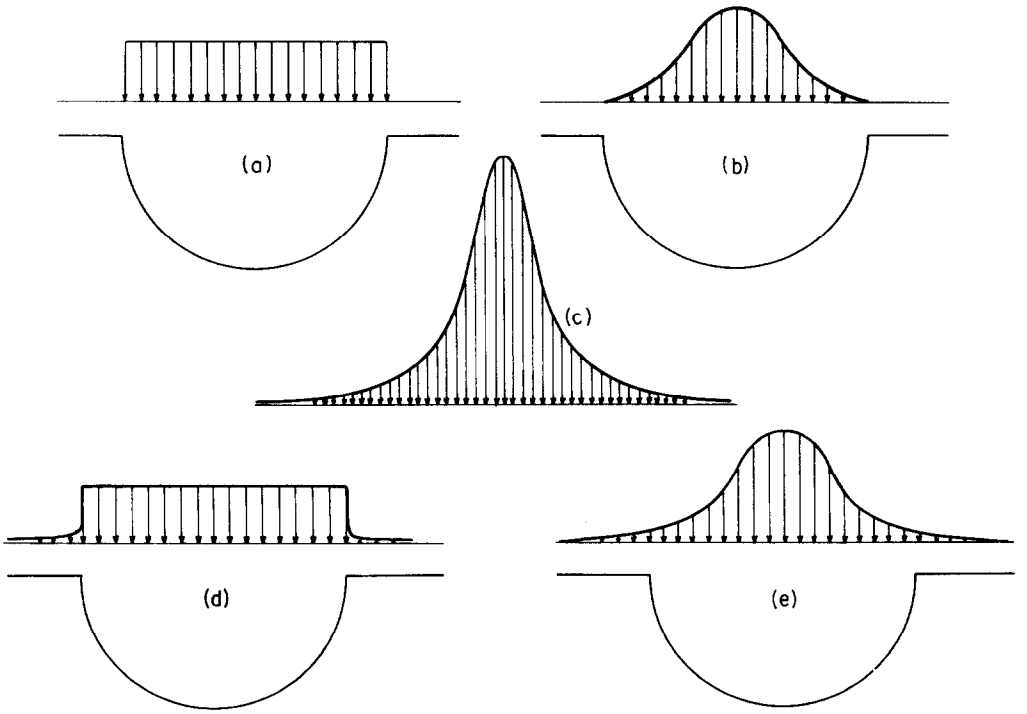

FIG. 2. Heat flux distributions (cavity enlarged for clarity).

varies according to the Gaussian distribution [4]:

$$q(r) = (3Q/\pi r_{ch}^2) \exp[-3(r/r_{ch})^2]$$

where r_{ch} is a characteristic radius. Over the interval $0 < r < r_{ch}$, 95% of the power is transferred.

(d) Distributed heat flux acting over a large surface with a constant value over a small cavity [cf. Fig. 2, case (d)]. In addition, outside the cavity the heat flux varies according to the Gaussian distribution given in case (c).

(e) Distributed heat flux acting over a large surface with a non-uniform distribution over a small cavity [cf. Fig. 2, case (e)]. This case considers the heat flux to vary with the cosine of the angle within the cavity and with a Gaussian distribution outside the cavity.

2.2. The thermal conductivities of the solid and the liquid are different but are independent of the temperature. Heat transfer is permitted in the radial, r, and colatitude, θ, directions with azimuthal symmetry.

2.3. Three different power levels were chosen to compare with the data of Landram [6].

2.4. The metal is considered to undergo a solid–liquid phase change. Since lead is a pure metal the phase change is assumed to take place with the latent heat being absorbed isothermally.

2.5. The heat transfer in the liquid phase is assumed to occur through conduction.

2.6. It is assumed that evaporation losses occur from the liquid metal surface outside the cavity, $r > r_i$. In this paper the term 'evaporation loss' is used for the energy loss accompanying the phase change of the liquid to the vapor when the liquid is below the boiling temperature.

2.7. At the boiling temperature one assumes that pool boiling occurs and that the liquid metal undergoes a liquid–vapor phase change at the constant temperature T_{boil}. Losses accompanying this phase change are referred to as boiling losses. It is assumed that once the boiling temperature is reached the heat is isothermally absorbed and that a mass of lead is lost through boiling at a rate determined by the heat input and the latent heat of vaporization. It is assumed that the loss of metal causes a spherical cavity to be formed, and the heat input is assumed to act on this surface. The calculation domain is then extended; i.e. the outer radius of the entire hemisphere is increased and the domain is remeshed accordingly.

2.8. The boundary of the solid of radius $r = R$ is assumed to be an adiabatic hemisphere which increases when a cavity forms due to boiling. The surface at $\theta = \pi/2$ outside the cavity, $r > r_i$, loses energy by radiation.

2.9. Initially, the metal is at the ambient temperature T_i.

3. MATHEMATICAL MODEL

The governing energy equation and boundary conditions and the formulation of the phase change relations are now presented.

3.1. *Governing differential equation and conditions*

The two-dimensional heat conduction equation is written in spherical coordinates as follows

$$\rho c_p \, \partial T/\partial t = (1/r^2) \, \partial/\partial r(kr^2 \, \partial T/\partial r) + 1/(r^2 \sin\theta) \, \partial/\partial\theta(k \sin\theta \, \partial T/\partial\theta). \quad (1)$$

The initial condition is given by

$$T(r, \theta) = T_i = \text{constant}. \quad (2)$$

The adiabatic boundary condition at $r = R$ is

$$\partial T/\partial r = 0 \quad 0 \leqslant \theta \leqslant \pi/2, \quad r = R. \quad (3)$$

On the small cavity of radius r_i on the upper surface

$$-k \, \partial T/\partial r = q(\theta) \quad 0 \leqslant \theta \leqslant \pi/2, \quad r = r_i. \quad (4)$$

Over the plane surface external to the cavity,

$$\theta = \pi/2, \quad r_i < r < R$$

we have

$$k/r \, \partial T/\partial\theta = q(r) - q_{rad} - q_{evap}, \quad \theta = \pi/2, \quad r_i < r < R. \quad (5)$$

The heat inputs $q(\theta)$ and $q(r)$ are given by:

(a) concentrated uniform flux with a cavity:

$$q(\theta) = Q/2\pi r_i^2, \quad q(r) = 0 \quad \text{for} \quad r > r_i. \quad (6a)$$

(b) concentrated non-uniform flux with a cavity:

$$q(\theta) = Q \cos\theta/\pi r_i^2, \quad q(r) = 0 \quad \text{for} \quad r > r_i. \quad (6b)$$

(c) distributed flux without a cavity:

$$q(r) = (3Q/\pi r_{ch}^2) \exp[-3(r/r_{ch})^2], \quad 0 < r < R. \quad (6c)$$

(d) distributed flux with a cavity:

$$q(\theta) = (Q/2\pi r_i^2)\{1 - \exp[-3(r_i/r_{ch})^2]\}. \quad (6d)$$

(e) distributed flux with a cavity (cosine distribution):

$$q(\theta) = (Q/\pi r_i^2)\{1 - \exp[-3(r_i/r_{ch})^2]\} \cos\theta. \quad (6e)$$

Cases (d) and (e) have

$$q(r) = 3Q/\pi r_{ch}^2 \exp[-3(r/r_{ch})^2]. \quad (6f)$$

The total or integrated power is the same at a given power level for all five cases. The value used for r_{ch} is 2 mm [5]. The values of r_i vary with time. The initial values are $r_i = \Delta r/2$ for cases (a) and (b) and $r_i = r_{ch}$ for cases (d) and (e). In equation (5)

$$q_{rad} = \varepsilon\sigma[T^4(r, \pi/2) - T_\infty^4],$$

and $q_{evap} = Wh_{fg}$ when $T(r, \pi/2) > T_{melt}$. W is the evaporation flux which is obtained from the relation [8, 13]

$$\log W = A - B/T - 1/2 \log T + C. \quad (7)$$

The above equation is specified for vacuum conditions but was used for the present study. The constants are specified in the nomenclature.

3.2. *Interface conditions*

The effect of melting is calculated by the following method proposed by Dusinberre [9] and modified by Doherty and Lachenbruch (cf. [10]). Melting begins when the temperature, T_{calc}, is greater than the melting temperature. The energy $Q = \rho c_p \Delta V(T_{calc} - T_{melt})$ is then determined. If this quantity is less than the latent heat of fusion, $\rho \Delta V h_{fus}$, the temperature T_{calc} is reset to T_{melt} and the calculations are repeated. When the sum of the Qs exceeds the latent heat, the phase change for the zone is assumed to be completed. The temperature of the liquid exceeds the fusion temperature by the amount $\Delta T = (Q - \rho \Delta V h_{fus})/\rho c_p \Delta V$. The exact melt surface boundary condition has been derived by Patel [14] and used by Lazaridis [15] in finite-difference calculations. As noted above the present method uses a small finite control volume which is heated until the energy absorbed is equal to the latent heat of fusion. This energy balance permits variations in the angular direction, θ. This method was chosen so that boiling could be included both in this analysis and in the future analyses for three-dimensional variations with a moving heat source; comparisons with other investigators are given at the end of Section 4.

As noted above, boiling in the liquid has also been considered. Boiling is assumed to occur when the calculated temperature is greater than the boiling temperature. The quantity $Q = \rho c_p \Delta V(T_{calc} - T_{boil})$ is then calculated and the mass Δm that is boiled and lost to the surroundings is obtained from $Q = \Delta m h_{fg}$. The temperature T_{calc} is then reset to T_{boil}. A new cavity size is then calculated according to $r_{in}^3 = r_i^3 + 3\Delta m/2\pi\rho$ where r_{in} is the new radius of the small cavity. The outer radius R is then increased to a larger value R_n according to $R - r_i = R_n - r_{in}$ and the grid arrangement is changed accordingly. Temperatures at the new nodal points are recalculated based on an energy balance for the new control volumes. The calculations are then repeated.

4. NUMERICAL METHOD

The governing differential equation was written in finite-difference form and solved using two different numerical methods; namely an explicit method and an Alternating Direction Implicit (ADI) method. The explicit method is relatively straightforward but requires large amounts of computing time because of the stringent Courant stability condition which is expressed as $\Delta t \leqslant (\rho c/2k)(\Delta r)^2/[1 + (\Delta r)^2/(r\Delta\theta)^2]$ for internal nodes. In this study the minimum time step used is 0.001 s and about 300 c.p.u. min are required on a VAX 11/750 for 16 s of arc heating. The large computer time makes the use of more efficient, implicit or semi-implicit methods desirable and therefore the ADI method was also used. This method solves the two-dimensional problem by solving one direction explicitly and the other implicitly in the first half time step. This is then reversed in the next time step. If the two equations are considered separately, they are only conditionally stable, but the combination of the two equations is unconditionally stable. The equations for the two methods are given in the Appendix. The calculation domain is illustrated in Fig. 1.

The program was compared with analytical solutions in the absence of phase change, and excellent agreement was obtained. Comparison was also made between the explicit and the implicit solutions. The maximum difference between the results is 3% at the initial stage of the computation and decreases to about 0.05% at later times. Comparison of the explicit method with the ADI method showed excellent agreement for the completion of fusion. However, for the case of ice melting with small temperature differences in the system, the ADI method does not give good results for predicting the beginning of melting. This is caused by the simultaneous implicit half time step approach (noted above) which may produce temperatures that are above the melting temperature at several nodal points simultaneously. This problem does not arise from the present work because large temperature differences are characteristic to the process.

Time step and mesh sensitivity analyses were undertaken. The temperature distribution away from the cavity showed little dependence on mesh size for values of Δr (mm) equal to 1.1206, 0.7620 and 0.6145. Near the cavity the temperature was dependent on the mesh size which resulted in a maximum variation of 6%. For time steps, Δt, of 0.003 s and less there is virtually no variation. It is also noted that Hsu and Rubinsky [11] checked the results by utilizing the temperatures in the solid to obtain the weld penetration by an inverse method. The agreement between the two results was very good. In addition, comparisons were made with other reported results for the interface location as a function of time. In a symmetrical square geometry, results for the interface location along the diagonal and along the adiabatic surface are presented by Rao and Sastri [16]. These also include the results of Lazaridis [15], Crowley [17], and Rathjen and Jiji [18]. The present method gave results that were in very good agreement with their studies.

5. RESULTS AND DISCUSSION

The fusion boundary penetration depth, temperature distribution and energy distribution were determined for different power levels and power distributions. Representative results are presented and discussed.

5.1. *Fusion boundary penetration*

Numerical results for the fusion boundary penetration depth are shown in Fig. 3(a) at $\theta = 8.18°$ for three different power levels. The calculations are for case (b); i.e. a concentrated heat flux acting non-uniformly over a small cavity. Landram's data [6] at $\theta = 0$ are also presented on the figure. It is seen that at the low power

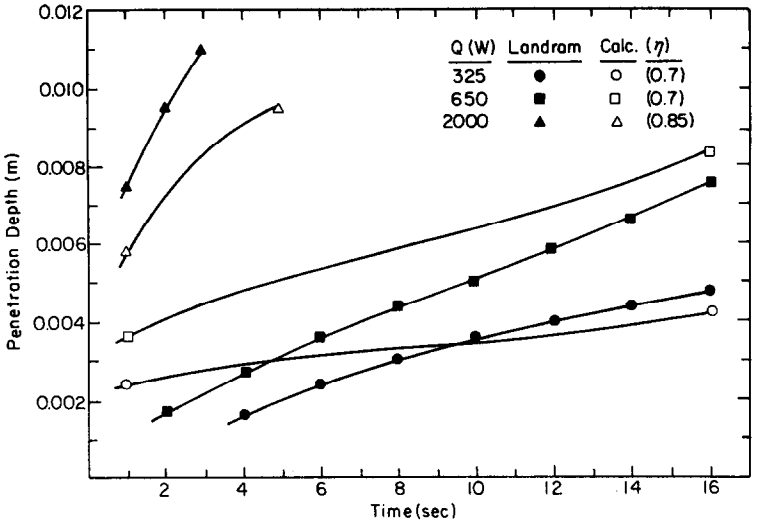

FIG. 3(a). Penetration depth. Data at $\theta = 0°$. Calculation at $\theta = 8.18°$. Case (b), concentrated cosine variation over small cavity.

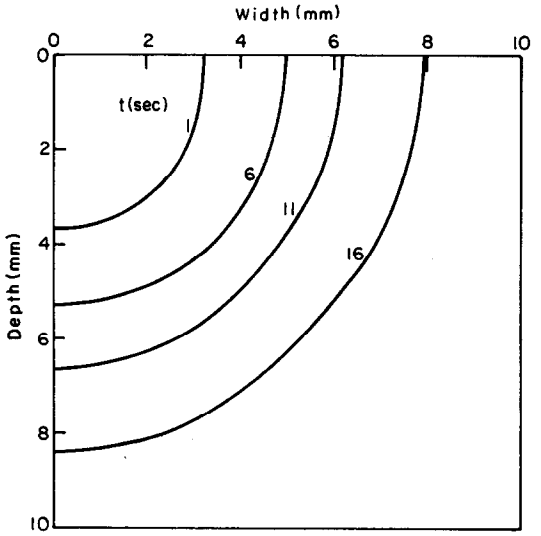

FIG. 3(b). Penetration location. $Q = 650$ W, $\eta = 0.7$. Case (b), concentrated cosine variation over small cavity.

levels of 325 and 650 W* there is reasonable agreement between the calculations and the experimental data. This is not true at the high power level of 2000 W.

One can observe a significant increase of the penetration with respect to the power level. Note that the computed values are not supposed to pass through zero because of the presence of an initial cavity. With respect to the experimental data close to the origin, difficulties exist in obtaining data during the early stage of the process by the inverse conduction method.

* For this case the loci of the interface are shown in Fig. 3(b) at several times as melting progresses.

The agreement of the computational results with the experimental data is certainly reasonable in view of the difficulties mentioned and the simplifying assumptions that the analysis is based on. The most important simplification is probably that of constant power as a function of time. However, at the end of the welding period the agreement between the experimental and the theoretical penetration is good, differing by less than 1 mm for the lower power levels. At the 2000 W power level the experimental penetration depth exhibits a significantly larger slope than the computed depth. This may be due to a considerable increase in convective effects in the liquid phase at very large power levels.

5.2. *Fusion boundary penetration for different power distributions*

The effect of power distribution on the fusion boundary penetration was examined for different power levels. Figures 4(a)–(c) show the variation of the penetration depth for different power distributions. Both the concentrated and distributed powers with a cavity give reasonable agreement with the experimental data especially at larger times.

One can conclude that the distributed flux without a cavity is not a suitable simulation of the power distribution for lead because these calculations yield a wide liquid metal pool of small depth which is contrary to the experimental evidence. It is also likely that the cosine power distribution in the cavity is better than the uniform distribution despite the fact that this statement seems to slightly contradict the results that are shown in Fig. 4(a). This statement is based on the result that the cosine power distribution gives a penetration depth which is deeper in the vertical direction than in the horizontal direction (an elongated pool shape) which is in agreement with all the experimental evidence.

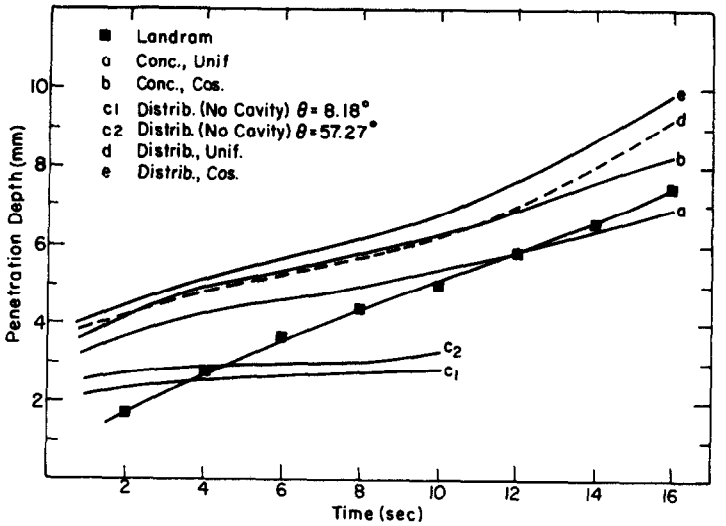

FIG. 4(a). Penetration depth. $Q = 650$ W, $\eta = 0.7$. Data at $\theta = 0°$. Calculations c1 at $\theta = 8.18°$ and c2 at $\theta = 57.27°$.

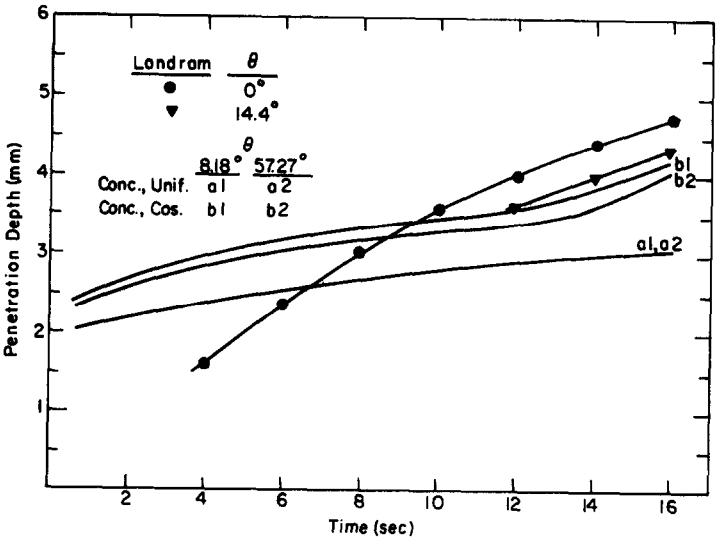

FIG. 4(b). Penetration depth. $Q = 325$ W, $\eta = 0.7$. Angular variation for concentrated flux conditions (a) and (b).

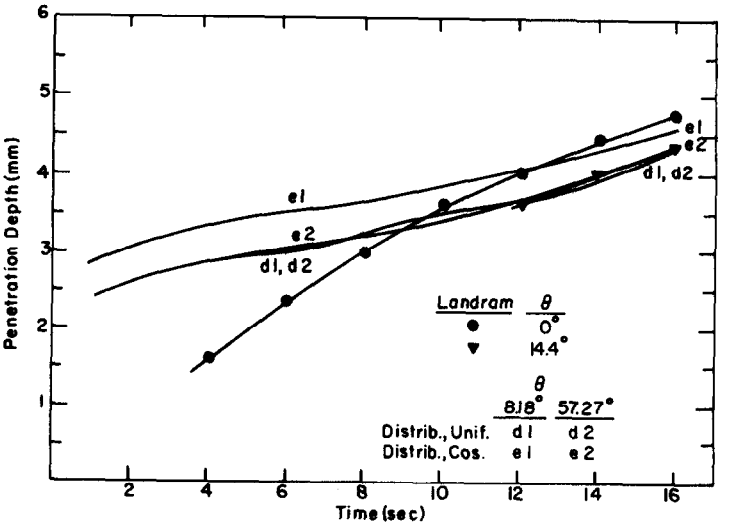

FIG. 4(c). Penetration depth. $Q = 325$ W, $\eta = 0.7$. Angular variation for distributed flux conditions (d) and (e).

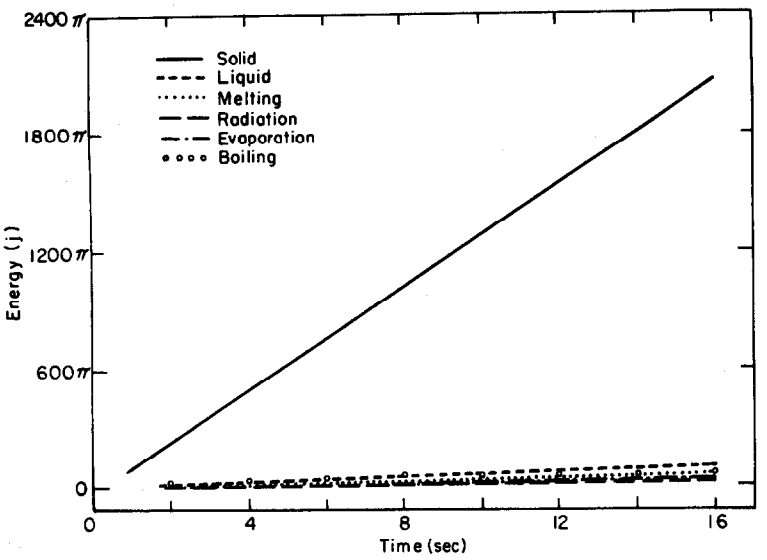

FIG. 5(a). Energy contributions. $Q = 650$ W, $\eta = 0.7$. Case (b) concentrated cosine variation over small cavity.

The results for the fusion boundary penetration suggest that it is likely that for lead (and for other low fusion temperature materials) that the arc quickly forms a cavity as a consequence of the very high local temperature and the associated loss of mass. The arc predominantly affects the bottom of the cavity thereby leading to a deep cavity. It is emphasized that this conclusion is considered to be valid for low fusion temperature materials and a different behavior is anticipated when high fusion temperature materials are investigated which are accompanied by little mass loss.

5.3. *Energy balance during the welding process*

An energy balance was made at different power levels and distributions and is shown in Figs. 5(a) and (b). The contributions are defined as follows:

(a) Energy in the solid phase

$$Q_s = \int_0^t \left[\int_{V_s(t)} \rho c_{ps}(T - T_i)\, dV \right] dt$$

where $V_s(t)$ is the volume of the solid phase.

(b) Energy in the liquid phase

$$Q_L = \int_0^t \left[\int_{V_L(t)} \rho c_{PL}(T - T_{fus})\, dV \right] dt$$

where $V_L(t)$ is the volume of the liquid phase.

(c) Latent heat of fusion

$$Q_{fus} = \int_0^t \left[\int_{A_{fus}} \rho (d\delta/dt) h_{fus}\, dA \right] dt$$

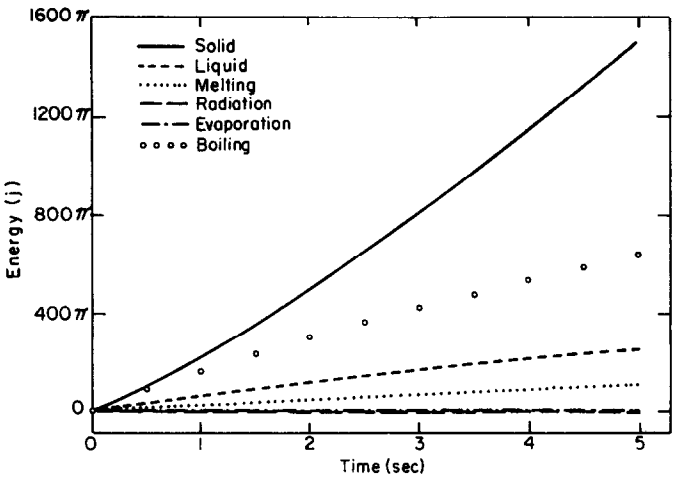

FIG. 5(b). Energy contributions. $Q = 2000$ W. $\eta = 0.85$. Case (b), concentrated cosine variation over small cavity.

where $A_{fus}(t)$ is the area of the fusion boundary and $\delta(t)$ is the penetration depth.

(d) Energy loss due to radiation

$$Q_{rad} = \int_0^t \left[\int_{A_s} \varepsilon\sigma(T^4 - T_i^4)\, dA \right] dt$$

where A_s is the area of the flat surface $\theta = \pi/2$ outside the small cavity.

(e) Energy loss due to evaporation

$$Q_e = \int_0^t \left[\int_{A_s} W h_{fg}\, dA \right] dt.$$

where W is the rate of evaporation. This loss occurs at the liquid surface when the temperature is below the boiling temperature.

(f) Energy loss due to boiling

$$Q_b = \int_0^t \Delta m h_{fg}\, dt$$

where Δm is the mass loss due to boiling.

From Figs. 5(a) and (b) it is seen that the dominant contribution is the accumulation of the energy in the solid. At 650 W the other quantities are negligible. For the high power input of $Q = 2000$ W, boiling and the energy content in the liquid are also important [cf. Fig. 5(b)]. At higher power levels boiling is expected to be considerably more important for low fusion and low boiling temperature materials. The energy in the liquid is related to the superheat above the melting temperature. At high power inputs the liquid is at temperatures significantly greater than the fusion temperature. It is also noted that at this condition the large temperature differences that are present probably cause increased fluid motion to occur in the liquid due to buoyancy and surface tension.

The radiation loss increases with increasing power levels but the contribution is very small in comparison to the other modes. The energy contribution related to the latent heat of fusion is numerically the same for the same depth of penetration. This contribution is also small.

The energy loss from evaporation as calculated from equation (6e) is also small. This contribution is sensitive to the power distribution and this will be presented later.

The strong dominance of the energy content in the solid phase as compared to the other modes explains why many simplified theoretical analyses, based only on conduction in the solid, sometimes provide reasonable approximate results for the welding process.

The energy loss by evaporation is shown in Fig. 6(a) for four different power distributions at $Q = 650$ W. The loss is largest for the concentrated flux acting uniformly over a small cavity, case (a). This is because this case results in the highest surface temperature ($\theta = \pi/2$) which yields the largest rate of evaporation.

The energy loss by boiling is shown in Fig. 6(b) for four different power distributions at $Q = 650$ W. This loss is largest for the concentrated flux acting non-uniformly over a small cavity, case (b). Note that this case yields the highest temperature within the cavity (at $\theta = 0$) which results in the largest boiling loss. Comparing the cases of distributed heat flux acting on a large surface the boiling loss is greater for the non-uniform [case (e)] than for the uniform [case (d)] distribution over a small cavity. The temperature at the bottom of the cavity is larger for case (e) than for case (d). It is noted that once boiling begins the temperature is assumed to remain at the saturation temperature.

The energy in the liquid phase is shown in Fig. 6(c) for four different power distributions at $Q = 650$ W. These results are consistent with the variations of the penetration depth in Fig. 4(a); i.e. the largest depths have the largest energies in the liquid region. The results show that the distributed heat fluxes, cases (d) and (e) yield more energy in the liquid phase than the concentrated heat fluxes, cases (a) and (b), respectively. Furthermore, the results for both non-uniform distributions over the small cavity; i.e. cases (b) and (c), yield more energy in the liquid phase than the uniform distributions, cases (a) and (d), respectively. This is consistent with the results of Figs. 6(a) and (b) which show that the largest total energy loss from both evaporation and boiling corresponds, in turn, to the smallest energy in the liquid phase. Furthermore, it is emphasized that the losses are largest for case (a) [cf. Fig. 6(a)].

5.4. *Mass loss due to boiling and evaporation*

The mass loss due to boiling and evaporation is shown in Fig. 7 for the concentrated heat flux acting non-uniformly over a small cavity, case (b). The losses increase for increases in the power level.

At 2000 W the boiling mass loss is approx. 100 times greater than the evaporation loss. At this high power level a rapid increase of the liquid temperature occurs leading to significant boiling loss. The results at 650 W are similar but now the boiling mass loss is about 10 times the evaporation mass loss. At the low power level of 325 W a significant proportion of the liquid never reaches the boiling temperature and therefore the evaporation loss now exceeds that resulting from boiling. It is noted that only the mass change due to boiling was included in the calculation of the cavity. The loss due to surface evaporation is significant at low power levels, but in that case the total loss of mass is not significant.

Recall that at the lower power level the energy loss due to evaporation was greater than that due to boiling but both were still negligible with respect to the total energy balance [cf. Fig. 5(a)]. At the higher power level the energy loss due to boiling is very important and cannot be neglected. It is again emphasized that these results are only applicable to low boiling temperature and low fusion materials.

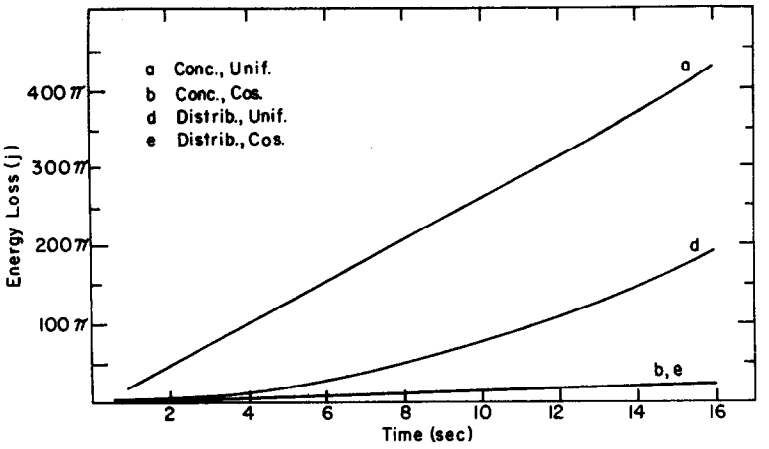

FIG. 6(a). Evaporation energy loss. $Q = 650$ W, $\eta = 0.7$.

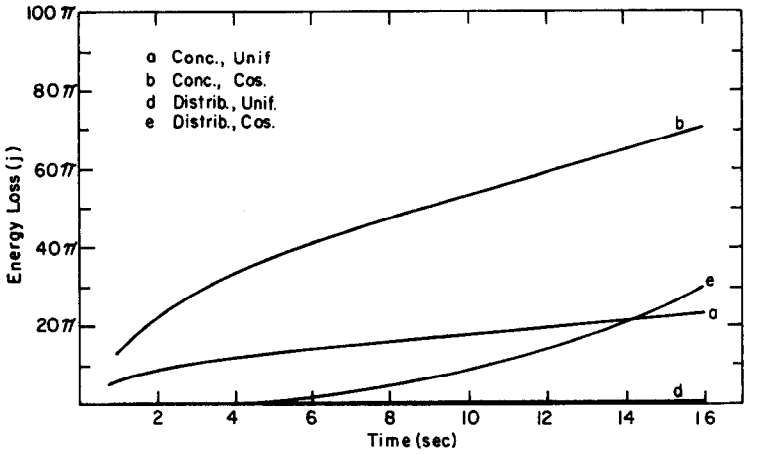

FIG. 6(b). Boiling energy loss. $Q = 650$ W, $\eta = 0.7$.

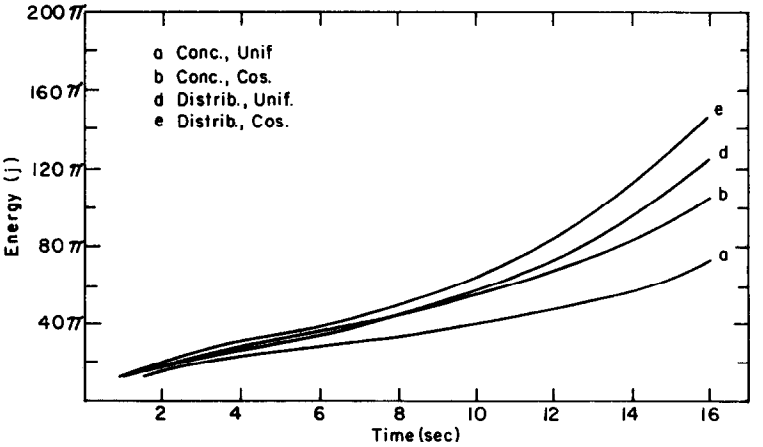

FIG. 6(c). Energy in liquid. $Q = 650$ W, $\eta = 0.7$.

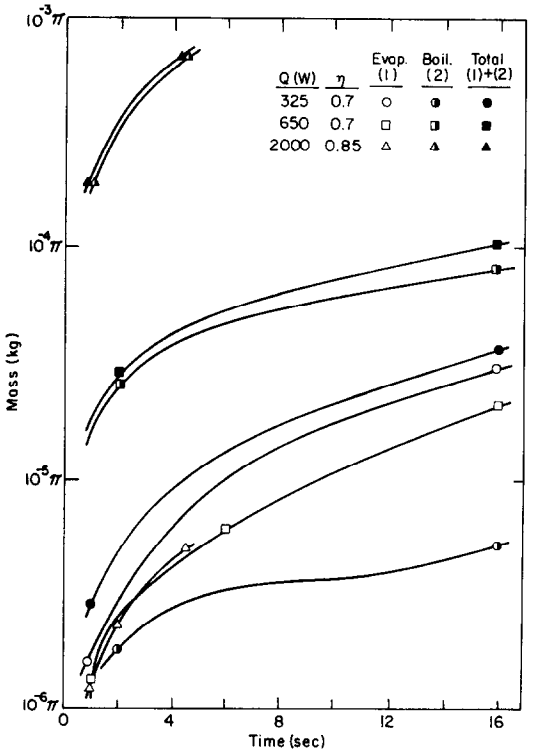

FIG. 7. Mass loss. Case (b), concentrated cosine variation over small cavity. Initial mass = 0.164 kg.

6. CONCLUSIONS

A study has been made for the heating of a material which experiences a change of phase. Gas tungsten arc welding of lead, a low boiling temperature and low fusion material is considered. The finite-difference program applicable to spherical coordinates, is two-dimensional with azimuthal symmetry and includes the effects of conduction, radiation, evaporation and boiling.

The calculated penetration depths are in good agreement with the experimental data at later times for 325 and 650 W power levels. At the large power level of 2000 W the experimental penetration speed is larger than the calculated speed. This may be due to fluid motion which is not included in this analysis.

For all the cases studied the energy content in the solid represents the largest contribution. At the high power level of 2000 W boiling is next in importance. At the low power levels the boiling, as well as evaporation energies are very small. The concentrated heat flux acting non-uniformly over a small cavity produced reasonable agreement with the experimental data for the penetration depth at all power levels.

Different power distributions were investigated and it was concluded that for low fusion temperature materials it is likely that the arc forms a cavity at the early stage of the process.

The arc predominantly affects the bottom of the cavity which leads to a deep pool; i.e. the maximum dimension is in the vertical direction as observed experimentally.

Heat balances were carried out and it was shown that the relative importance of different heat transfer modes depends strongly on the power level and distribution. However, the heat content of the solid phase remains dominant and this explains the relative success of some simplified analytical models in predicting fusion boundary penetration in the welding process.

A better simulation of the welding process would include fluid motion as this transport is likely to be significant especially at larger power levels. The scope of the work is presently being extended to high fusion temperature materials.

Acknowledgement—The authors would like to express their appreciation for the contributions by E. Lee, A. Mertol, and A. Mashaie. The support and assistance from Dr K. Mahin of Lawrence Livermore National Laboratory, Sandia National Laboratories, Livermore, and Energy Mines and Resources, Canada is gratefully acknowledged.

REFERENCES

1. H. D. Brody and D. Apelian (Editors), *Modeling of Casting and Welding Processes*. Metallurgical Society of AIME, PA (1981).
2. S. A. David (Editor), *Trends in Welding Research in the United Sates*. American Society for Metals, OH (1982).
3. M. M. Chen, J. Mazumder and C. Tucker (Editors), *Transport Phenomena in Materials Processing*. AIME, PED-Vol. 10, HTD-Vol. 29 (1983).
4. S. S. Glickstein and E. Friedman, Temperature transients in gas tungsten arc weldments, *Weld. Rev.* 72–76 (May 1983).
5. S. S. Glickstein and E. Friedman, Weld modeling applications, *Weld. J.* **63**, 38–42 (September 1984).
6. C. S. Landram, Measurement of fusion-boundary energy transport during arc welding, *Trans. Am. Soc. Mech. Engrs*, Series C, *J. Heat Transfer* **105**, 550–554 (1983).
7. J. G. Andrews and D. R. Atthey, The response of a weld pool to perturbation in power, *Int. Journal Heat Mass Transfer* **22**, 1533–1538 (1979).
8. S. Dushman and J. M. Lafferty, *Scientific Foundations of Vacuum Technique*, 2nd edn, pp. 691–731. John Wiley, New York (1962).
9. G. M. Dusinberre, *Heat Transfer Calculations by Finite Difference*. International Textbook, Pennsylvania (1961).
10. V. J. Lunardini, *Heat Transfer in Cold Climates*, p. 495. Van Nostrand Reinhold, New York (1981).
11. Y. Hsu and B. Rubinsky, Private communication (1985).
12. M. Salcudean and C. H. Low, Mathematical modelling of heat transfer in permanent molds, Report to Energy Mines and Resources, Canada (1982).
13. D. E. Gray, *American Institute of Physics Handbook*, 3rd edn, pp. 4–222, 4–315. McGraw-Hill, New York (1972).
14. P. D. Patel, Interface conditions in heat-conduction problems with change of phase, *AIAA Jl* **6**, 2454 (1968).
15. A. Lazaridis, A numerical solution of the multidimensional solidification problem, *Int. J. Heat Mass Transfer* **13**, 1459–1477 (1970).
16. P. R. Rao and V. M. K. Sastri, Efficient numerical method for two dimensional phase change problems, *Int. J. Heat Mass Transfer* **27**, 2077–2084 (1984).
17. A. B. Crowley, Numerical solution of Stefan problems, *Int. J. Heat Mass Transfer* **21**, 215–219 (1978).
18. K. A. Rathjen and L. M. Jiji, Heat conduction with melting or freezing in a corner, *Trans. Am. Soc. mech. Engrs*, Series C, *J. Heat Transfer* **93**, 101–109 (1971).

APPENDIX

For the explicit method the finite-difference relation reduces to

$$T_{i,j}^{n+1} = T_{i,j}^{n} + E\cdot(A+B+C+D)$$

where

$$E = \frac{\Delta t}{\rho C_p r^2 \sin\theta\cdot\Delta r\cdot\Delta\theta}$$

$$A = k_{i,j+1/2}(T_{i,j+1}^{n} - T_{i,j}^{n})\cdot\sin\left(\theta+\frac{\Delta\theta}{2}\right)\cdot\Delta r/\Delta\theta$$

$$B = k_{i,j-1/2}(T_{i,j-1}^{n} - T_{i,j}^{n})\cdot\sin\left(\theta-\frac{\Delta\theta}{2}\right)\cdot\Delta r/\Delta\theta$$

$$C = k_{i-1/2,j}(T_{i-1,j}^{n} - T_{i,j}^{n})\cdot\left(r-\frac{\Delta r}{2}\right)^2\sin\theta\cdot\frac{\Delta\theta}{\Delta r}$$

$$D = k_{i+1/2,j}(T_{i+1,j}^{n} - T_{i,j}^{n})\cdot\left(r+\frac{\Delta r}{2}\right)^2\sin\theta\cdot\frac{\Delta\theta}{\Delta r}.$$

For the ADI method the finite-difference form reduces to:

('r direction', implicit)

$$aT_{i-1,j}^{n+1/2} + bT_{i,j}^{n+1/2} + cT_{i+1,j}^{n+1/2} = d$$

$$a = -k_{i-1/2,j}\left(r-\frac{\Delta r}{2}\right)^2\Big/(r\Delta r)^2$$

$$b = \frac{\rho C_p}{\Delta t} + \left[k_{i-1/2,j}\left(r-\frac{\Delta r}{2}\right)^2 + k_{i+1/2,j}\left(r+\frac{\Delta r}{2}\right)^2\right]\Big/(r\Delta r)^2$$

$$c = -k_{i+1/2,j}\left(r+\frac{\Delta r}{2}\right)^2\Big/(r\Delta r)^2$$

$$d = \left\{\left(\frac{\rho C_p}{\Delta t} - \left[k_{i,j+1/2}\sin\left(\theta+\frac{\Delta\theta}{2}\right) + k_{i,j-1/2}\sin\left(\theta-\frac{\Delta\theta}{2}\right)\right]\Big/(r\Delta\theta)^2\sin\theta\right\}T_{i,j}^{n} + k_{i,j-1/2}T_{i,j-1}^{n}\sin\left(\theta-\frac{\Delta\theta}{2}\right)\Big/(r\Delta\theta)^2\sin\theta + k_{i,j+1/2}T_{i,j+1}^{n}\sin\left(\theta+\frac{\Delta\theta}{2}\right)\Big/(r\Delta\theta)^2\sin\theta.$$

('θ direction' implicit)

$$aT_{i,j-1}^{n+1} + bT_{i,j}^{n+1} + cT_{i,j+1}^{n+1} = d$$

where

$$a = -k_{i,j-1/2}\sin\left(\theta-\frac{\Delta\theta}{2}\right)\Big/(r\Delta\theta)^2\sin\theta$$

$$b = \frac{\rho C_p}{\Delta t} + \left[k_{i,j-1/2}\sin\left(\theta-\frac{\Delta\theta}{2}\right) + k_{i,j+1/2}\sin\left(\theta+\frac{\Delta\theta}{2}\right)\right]\Big/(r\Delta\theta)^2\sin\theta$$

$$c = -k_{i,j+1/2}\sin\left(\theta+\frac{\Delta\theta}{2}\right)\Big/(r\Delta\theta)^2\sin\theta$$

$$d = \left\{\frac{\rho C_p}{\Delta t} - \left[k_{i+1/2,j}\left(r+\frac{\Delta r}{2}\right)^2 + k_{i-1/2,j}\left(r-\frac{\Delta r}{2}\right)^2\right]\Big/(r\Delta r)^2\right\}\times T_{i,j}^{n+1/2} + k_{i-1/2,j}T_{i-1,j}^{n+1/2}\left(r-\frac{\Delta r}{2}\right)^2\Big/(r\Delta r)^2 + k_{i+1/2,j}T_{i+1,j}^{n+1/2}\left(r+\frac{\Delta r}{2}\right)^2\Big/(r\Delta r)^2.$$

ETUDE DU TRANSFERT THERMIQUE PENDANT LE SOUDAGE A L'ARC

Résumé—On analyse le transfert de chaleur pendant le soudage. Les mécanismes de transfert thermique considérés incluent la conduction, le changement de phase solide–liquide, le changement de phase liquide–vapeur et le rayonnement. La profondeur de pénétration est calculée pour différents niveaux de puissance et plusieurs distributions et les résultats sont comparés aux données expérimenatles pour le plomb. La contribution et l'importance des différents modes de transfert thermique sont précisées.

UNTERSUCHUNG DES WÄRMETRANSPORTS BEIM LICHTBOGENSCHWEISSEN

Zusammenfassung—Es sind Berechnungen des Wärmeübergangs beim Lichtbogenschweißen durchgeführt worden. Neben der Wärmeleitung wurde der Wärmetransport beim Phasenwechsel fest–flüssig, beim Phasenwechsel (flüssig–gasförmig) und bei der Strahlung berücksichtigt. Die Einbrenntiefe wird für unterschiedliche Energiedichten und -verteilungen berechnet und die Ergebnisse mit experimentellen Daten von Blei verglichen. Die unterschiedlichen Wärmetransport-Mechanismen werden hinsichtlich ihres Beitrags und ihrer Bedeutung zum Gesamteffekt bewertet.

ИССЛЕДОВАНИЕ ТЕПЛООБМЕНА ПРИ ДУГОВОЙ СВАРКЕ

Аннотация—Проведен анализ теплообмена при дуговой сварке. Рассмотрены механизмы теплопереноса, включая кондукцию, фазовые переходы твердое тело–жидкость, жидкость–пар и излучение. Глубина проникновения рассчитывается для различных энергетических уровней и распределений, а результаты расчетов сравниваются с данными экспериментов, проведенных со свинцом. Оцениваются вклады и важность различных режимов теплообмена.